Modeling study of $PM_{2.5}$ pollution episode of early spring 2019 in Hokkaido, Japan caused by biomass burning in Northeast China

Katsushige Uranishi[1*,3], *Hikari* Shimadera[2], *Fumikazu* Ikemori[3], *Kyohei* Takami[4], *Atsushi* Nogami[1], and *Seiji* Sugata[5]

[1]Department of Life and Environment Engineering, The University of Kitakyushu, Kitakyushu, Japan
[2]Graduate School of Engineering, Division of Sustainable Energy and Environmental Engineering, Osaka University, Suita, Japan
[3]Nagoya City Institute for Environmental Sciences, Nagoya, Japan
[4]KANSO TECHNOS CO. LTD., Osaka, Japan
[5]National Institute for Environmental Studies, Tsukuba, Japan

Abstract. Biomass burning (BB), in particular agricultural waste burning (Agri-BB), occurs at random locations, scales, and times. These factors make it challenging to detect Agri-BB accurately through satellite observations. Thus, the BB emission inventories using satellite observation data have uncertainties for their emission estimation approach and cause poor model performance for air pollutants including $PM_{2.5}$. We utilized the two BB emission inventories, GFEDv4.1s and FINNv2.5 with the CMAQ model to simulate the $PM_{2.5}$ heavy pollution episode in Hokkaido 2019. To estimate Agri-BB contributions, we conducted three simulation cases for each BB emission inventory: with and without Agri-BB emission, and the boosted Agri-BB emission cases. The baseline simulation failed to capture the temporal and spatial variation patterns of $PM_{2.5}$. Meanwhile, the boosted Agri-BB case could show favorable performance for $PM_{2.5}$ concentrations. These results indicated that the two BB emission inventories underestimated Agri-BB emissions. In the two boosted Agri-BB cases, the $PM_{2.5}$ contributions from Agri-BB accounted for more than 50% during the episode. Moreover, high $PM_{2.5}$ emissions were found in Northeast China and its surrounding regions similar to the two boosted Agri-BB cases. Consequently, the results revealed that Agri-BB emissions during the episode were significantly derived from the agricultural areas in Northeast China.

1 Introduction

Biomass burning (BB) refers to the combustion of organic resources derived from living and dead vegetation. BB, such as forest fires and agricultural waste burning (hereinafter referred to as Agri-BB) has caused significant atmospheric pollution and health concerns worldwide [1-2]. Agri-BB is one of the anthropogenic BB and is widely practiced in Asian countries as

* Corresponding author: uranishi@kitakyu-u.ac.jp

© The Authors, published by EDP Sciences. This is an open access article distributed under the terms of the Creative Commons Attribution License 4.0 (https://creativecommons.org/licenses/by/4.0/).

part of agricultural activities due to its cost-effectiveness and convenience in waste disposal [3-5]. However, the timing of Agri-BB is difficult to determine accurately due to post-harvest season variations influenced by annual climate and weather patterns. Moreover, when extensive Agri-BB occurs within a short timeframe before planting, substantial air pollutants are released into the surrounding areas, which lead to haze formation and trigger respiratory and cardiovascular health issues [6-8]. This phenomenon has emerged as a critical issue in Asian countries such as China and India [6-8].

Northeast China is one of the major granaries in China and extensive BB events have been observed in the region. It is reported that the intensity of Agri-BB in Northeast China surpassed what has been observed in other regions [6] When an extensive Agri-BB event occurs during the post-harvest season and releases lots of air pollutants under stagnant weather conditions, it leads to severe haze events and exerts a myriad of impacts on regional air quality [9-10]. In addition, BB including Agri-BB in Northeast China partly contributed to the transboundary air pollution episode of autumn 2014 in the northern part (Rishiri Island) [11] and the central part (Noto peninsula) [12] of Japan. Hence, BB exerts damaging effects across various spatial scales from local to regional. Thus, it's important to understand how BB affects air quality in East Asia and suggest mitigation strategies to reduce its level. However, there are few studies simulating $PM_{2.5}$ transboundary pollution in Japan that originated from BB in Northeast China.

In Sapporo City, Hokkaido, Japan, hourly $PM_{2.5}$ concentration increased drastically from the 27th of February to the 3rd of March 2019, recording up to 200 μg/m^3 (hereinafter referred to as the $PM_{2.5}$ heavy pollution episode). In late February 2019, significant hotspots were observed in Northeast China and its surrounding regions via the Fire Information for Resource Management System (FIRMS, https://earthdata.nasa.gov/firms) (Figure 1). We reported that the boosted BB emission on the crop land was able to well reproduce daily $PM_{2.5}$ concentrations in Northeast China and Hokkaido, Japan during the PM2.5 heavy pollution episode using the Community Multiscale Air Quality (CMAQ) model and the Global Fire Assimilation System (GFAS). GFAS was the sole available global BB emission inventory in 2020 when we worked on our study [13]. The GFAS is a BB emission inventory converting fire radiative power (FRP) observations from MODIS satellites into smoke constituents [14]. However, the BB emission inventory does not provide BB emissions for different land use/cover categories (savanna, boreal forest, temperate forest, and agricultural land etc.). Therefore, it was not possible to accurately evaluate the $PM_{2.5}$ contribution from Agri-BB in Northeast China.

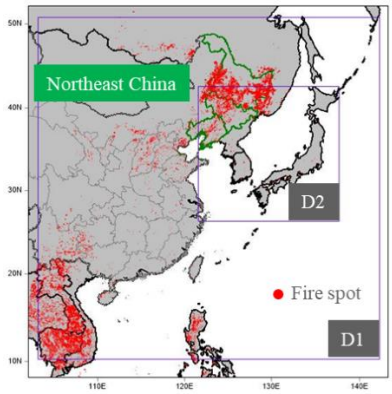

Fig. 1. Modeling domains for CMAQ and fire spots (MCD14DL) obtained from FIRMS during the $PM_{2.5}$ heavy pollution episode from the 27th of February to the 3rd of March in 2019. Green lines indicate Northeast China region in China.

On the other hand, both the Global Fire Emissions Database (GFED) [15] and the Fire INventory from NCAR (FINN) [16] are some of the available global BB emission inventories for air quality simulations and provide several types of BB emission for corresponding land use/cover categories. FINN calculates the dry matter burned using fire hotspot data to estimate the burned area, while GFED uses the burned area product for its calculations [17]. Moreover, GFED v4.1s includes newly burned area estimates with contributions from small fires, with boosted BB emissions in agricultural areas in Asia, including Northeast China [15]. Meanwhile, the latest version of FINN v2.5 utilizes active fire detections from the Visible Infrared Imaging Radiometer Suite (VIIRS) at 375 m spatial resolution to allow smaller fires such as Agri-BB to be included in the emission processing. Both emission inventories show similar temporal and spatial variations in $PM_{2.5}$. However, the quantities of total $PM_{2.5}$ emissions differ substantially because each BB inventory was developed with a different approach for emission estimation. Therefore, assessing the model performance with other BB emission inventories should be taken into consideration.

In this work, we utilized the two BB emission inventories, GFED v4.1s and FINN v2.5 with the CMAQ model to simulate the $PM_{2.5}$ heavy pollution episode and to evaluate the model performance as well as the Agri-BB contributions on $PM_{2.5}$ concentrations in Hokkaido, Japan.

2 Materials and Methods

CMAQ v5.2.1 was employed to simulate the $PM_{2.5}$ heavy pollution episode. Meteorological fields were prepared using version 3.9.1 of the Weather Research and Forecasting (WRF) model. Figure 1 shows the modeling domains from East Asia (D1: 45 × 45 km) to Japan (D2: 15 × 15 km). The vertical layers consisted of 34 sigma-pressure coordinate layers ranging from the surface to 100 hPa with the vertical middle height of the first layer. Table 1 summarizes configurations of WRF and CMAQ models. The details of chemistry and physics options are available in the documentation for the models.

The emission data for CMAQ simulations were derived from various emission inventories as shown in Table 1. In particular, BB emissions were from GFED v4.1s and FINN v2.5. It is assumed that BB emissions were uniformly distributed from the surface to the Planetary Boundary Layer (PBL) height in accordance with our previous study [13]. Note that there were differences between the simulation period and the reference years in the anthropogenic emission data available for the simulations. Therefore, the uncertainties associated with these differences may affect the CMAQ model performance.

In order to investigate the BB emission divergence between the two BB inventories and the influence of Agri-BB pollutants during the $PM_{2.5}$ heavy pollution episode, the following simulations with each BB emission inventory were executed for 2 months from the 1st February 2019 to the 31st March 2019 (hereinafter called to as the target period) with spin-up period of 10 days: (1) the baseline cases with regular BB emission (base_GFED and base_FINN), (2) GFED_Agri-BB10, a simulation case with 10 times boosted Agri-BB emission in GFED v4.1s, (3) FINN_Agri-BB05, a simulation case with 5 times boosted Agri-BB emission in FINN v2.5 so that the emission level is comparable with that GFED_Agri-BB10. An additional simulation without Agri-BB sources (noAgri-BB) was conducted to estimate the $PM_{2.5}$ contribution from Agri-BB sources.

For evaluation of the CMAQ model performance, the simulation results were compared to the ground-level $PM_{2.5}$ concentration data from 17 sites in Northeast China obtained from Air quality data of China (https://www.aqistudy.cn/historydata/index.php), and to the data from 14 sites in Hokkaido, Japan provided by Air pollution monitoring data of Japan (https://tenbou.nies.go.jp/download/). We used time-series comparison and the index of

agreement (IA). IA is a statistical measure to evaluate the model performance and varies between 0 and 1, where 1 indicates a perfect model performance [18].

Table 1. Model configurations for WRF and CMAQ

WRF configuration	
Meteorology Model	WRF v3.9.1
Geography data	USGS 30sec topography and land use (East Asia) MLIT-GIAJ land use (100m, Japan)
Analysis data	NCEP FNL, RTG_SST_HR
Explicit precipitation scheme	WRF Single–moment 6–class scheme
Radiation	RRTM scheme (long wave), Dudhia scheme (short wave)
Surface-layer option	Revised MM5 scheme
Land-surface	Noah Land-Surface Model
Planetary boundary layer scheme	Yonsei University scheme
Cumulus option	Kain-Fritsch sheme
FDDA	$G_{t,\,q,\,uv} = 3.0\times10^{-4}\ s^{-1}$ (D1, D2)
CMAQ configuration	
Chemistry Model	CMAQ v5.2.1
Emission	Asia: REAS v3.2.1 (2017), Japan: MOE PM2.5 EI (2015) & OPRF2010 (Ship), Biogenic: MEGANv2.04, Volcano: Aerocom, Biomass burning: GFED v4.1s or FINN v2.5,
Initial/Boundary concentrations	CAM-chem (D1)
Advection	Yamartino/WRF-based scheme, Multiscale/ACM2
Vertical diffusion	Asymmetrical Convective Model version 2 (ACM2)
CMAQ chemistry	SAPRC07 and AERO6 with Aqueous chemistry

3 Results and Discussions

3.1 Model simulation performance

Figure 2 shows the comparison of the results of baseline and boosted Agri-BB cases versus the observation data in terms of the mean concentrations and IA values of $PM_{2.5}$ during the target period. Compared to the two boosted Agri-BB cases (GFED_Agri-BB10 and FINN_Agri-BB05), both GFED_base and FINN_base cases showed relatively large differences between simulated and observed $PM_{2.5}$ concentrations in Northeast China and Hokkaido regions. Meanwhile, the favorable performance in the boosted Agri-BB cases was also supported by the higher IA values for the two regions (0.74 in GFED_Agri-BB10 case

and 0.76 in FINN_Agri-BB05 versus 0.65 in GFED_base and 0.72 in FINN_base). Figure 3 shows the comparison of the observed and simulated daily mean $PM_{2.5}$ concentrations during the target period in Hokkaido, Japan. The CMAQ model in the two boosted Agri-BB cases effectively simulated the day-to-day variation patterns for the site-averaged products in Hokkaido, including the occurrence of high concentration peaks around the 1st of March 2019. These results indicate that the two BB emission inventories (GFED v4.1s and FINN v2.5) underestimate Agri-BB emissions.

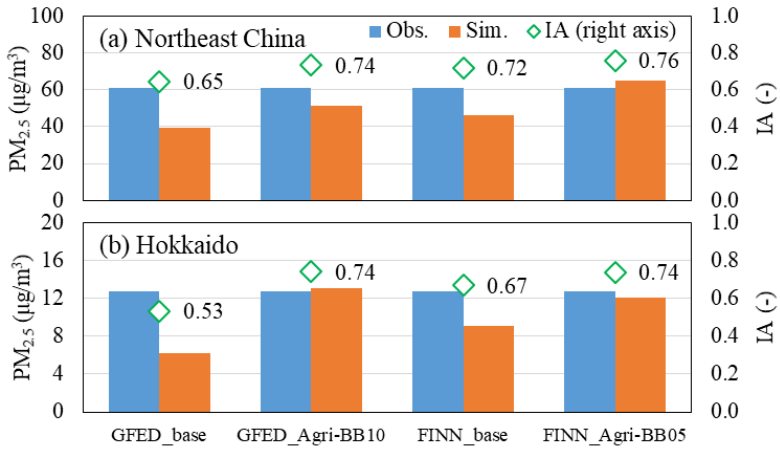

Fig. 2. Comparison of the results of baseline and boosted Agri-BB cases versus the observation data in terms of the mean concentrations and IA values of PM2.5 during the target period (from 1st Feb to 31st Mar 2019).

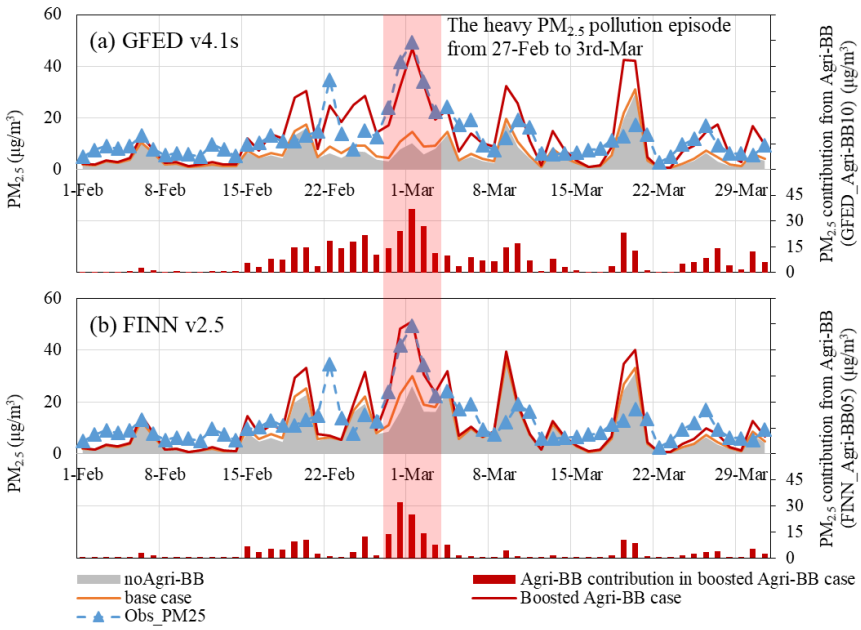

Fig. 3. Comparison of the observed and simulated daily mean $PM_{2.5}$ concentrations in the base, boosted Agri-BB, and noAgri-BB cases as well as $PM_{2.5}$ contributions in the boosted Agri-BB cases in Hokkaido, Japan

3.2 Agri-BB source analysis during the $PM_{2.5}$ heavy pollution episode

The Agri-BB contributions on $PM_{2.5}$ concentrations in Hokkaido in the two boosted Agri-BB cases were estimated during the target period as shown in Figure 3. The results in the two simulation cases were consistent in which the $PM_{2.5}$ contribution from Agri-BB was highest in Hokkaido during the PM2.5 heavy pollution episode (36.8 μg/m^3 on the 1st of March in GFED_Agri-BB10 and 32.1 μg/m^3 on the 28th of February in FINN_Agri-BB05) when the daily mean $PM_{2.5}$ concentration was maximum (46.9 μg/m^3 in GFED_Agri-BB10 and 51.3 μg/m^3 in FINN_Agri-BB05 versus 49.4 μg/m^3 as observed value), although trends of Agri-BB contributions in the two boosted Agri-BB cases differ in their day-to-day variation patterns due to differences of BB emission estimation approach between GFED v4.1s and FINN v2.5. In both cases, the $PM_{2.5}$ contribution from Agri-BB accounted for more than 50% during the $PM_{2.5}$ heavy pollution episode (66% in GFED_Agri-BB10 and 54% in FINN_Agri-BB05 cases), indicating that Agri-BB source was strongly involved in the episode.

Figure 4 shows the spatial distributions of mean $PM_{2.5}$ emissions from Agri-BB during the $PM_{2.5}$ heavy pollution episode in the two boosted Agri-BB cases. Both $PM_{2.5}$ emissions from Agri-BB have a similar spatial pattern to one another and show high spatial variation. In particular, high $PM_{2.5}$ emissions were found in Northeast China and its surrounding regions that are common with the two cases. These results illustrated that Agri-BB emissions during the $PM_{2.5}$ heavy pollution episode was substantially derived from agricultural area in Northeast China and also indicated that the $PM_{2.5}$ heavy pollution in Hokkaido 2019 was strongly affected by Agri-BB occurred in Northeast China. Meanwhile, it was found that the existing BB emission inventories, such as GFED v4.1s and FINN v2.5 were found to underestimate emissions from Agri-BB sources in Northeast China, since the boosted Agri-BB emission cases enable us to effectively reproduce daily $PM_{2.5}$ concentrations during the $PM_{2.5}$ heavy pollution episode.

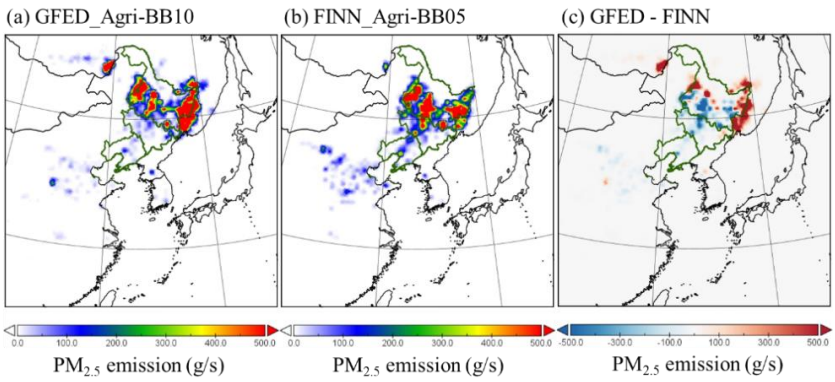

Fig. 4. The spatial distributions of mean $PM_{2.5}$ emissions from Agri-BB during the $PM_{2.5}$ heavy pollution episode: (a) GFED_Agri-BB10, (b) FINN_Agri-BB, and (c) GFED_Agri-BB10-FINN-FINN_Agri-BB05. Green lines indicate Northeast China region in China.

4 Conclusion

Agri-BB is a widespread practice to process crop residue in rural China and causes heavy air pollution from local to regional scales which significantly affects public health. This work investigated the $PM_{2.5}$ pollution episode in Hokkaido that occurred in early spring 2019 using the CMAQ model with the two BB emission inventories (GFED v4.1s and FINN v2.5). We also estimated Agri-BB impact during the heavy $PM_{2.5}$ pollution episode conducting three simulation cases for each BB emission inventory: with and without Agri-BB emission, and

the boosted Agri-BB emission cases. The CMAQ performance for regional transport of $PM_{2.5}$ concentrations was evaluated using ground-level observation data in Northeast China and Hokkaido, Japan. The model in the baseline cases failed to capture the temporal and spatial variation patterns of $PM_{2.5}$ mass during the $PM_{2.5}$ heavy pollution episode. Meanwhile, the model in the boosted Agri-BB cases were able to show a favorable performance for $PM_{2.5}$ concentrations during the whole simulation period, including $PM_{2.5}$ concentration spikes during the $PM_{2.5}$ heavy pollution episode. These results indicated that the two BB emission inventories (GFED v4.1s and FINN v2.5) underestimated Agri-BB emissions. Moreover, the Agri-BB contributions on $PM_{2.5}$ concentrations in Hokkaido in the two boosted Agri-BB cases were estimated during the target period for Agri-BB source analysis. The results in the two simulation cases were consistent in that the $PM_{2.5}$ contribution from Agri-BB was highest in Hokkaido during the $PM_{2.5}$ heavy pollution episode when the daily mean $PM_{2.5}$ concentration was maximum. In both cases, the $PM_{2.5}$ contribution from Agri-BB accounted for more than 50% during the $PM_{2.5}$ heavy pollution episode, indicating that Agri-BB source was strongly affected in the episode. During the episode, high $PM_{2.5}$ emissions were found in Northeast China and its surrounding regions that were common with the two cases. The result illustrated that Agri-BB emissions during the $PM_{2.5}$ heavy pollution episode was substantially derived from agricultural area in Northeast China. In addition, GFED v4.1s and FINN v2.5 were found to underestimate emissions from Agri-BB sources in Northeast China. Thus, in conducting simulations using existing BB emission inventories, it is necessary to consider substantial underestimation of Agri-BB emissions, specifically during harvesting and post-harvest seasons.

This research was conducted as Type II joint research of the National Institute for Environmental Studies (NIES) and environmental research institutes of local government in Japan. The computational resources were provided by NIES. We acknowledged the use of data and imagery from LANCE FIRMS operated by the NASA/GSFC/Earth Science Data and Information System (ESDIS) with funding provided by NASA/HQ.

References

1. Andreae M O and Merlet P 2001 Glob. Biogeochem. Cycles **15** 955-66
2. Chen J, Li C, Ristovski Z et al 2016 Sci. Total Environ. **579** 1000-34
3. Lasko K, Vadrevu K P and Ngruyen T T N 2018 Plos One **13** e0196629
4. Lasko K, Vadrevu K P, Tran V T and Justice C 2018 IEEE J. Sel. Top. Appl. Earth Obs. Remote Sens **11** 498-12
5. Lasko K and Vadrevu K P 2018 Environ. Pollut. **236** 795–06
6. Yin S, Wang X, Xiao Y, H. Tani H, Zhong G and Sun Z 2017 Environ. Pollut. **220** 204–21
7. Wang Z, Zhao J, Xu J, Jia M, Li H and Wang S 2019 Int. J. Environ. Res. **16** 1379
8. Vadrevu K P, Csiszar I, Ellicott E, Giglio L, Badarinath K V S, Vermote E and Justice C 2013 IEEE J. Sel. Top. Appl. Earth Obs. Remote Sens **6** 224-38
9. Wang H, An J, Shen L, Zhu B, Pan C, Liu Z, Wang Y 2014 Sci. Total Environ. **490** 501-08
10. Long X, Tie X, Cao J, Huang R, Feng T, Li N and Zhang, Q 2016 Atmos. Chem. Phys. **16** 9675-91
11. Zhu C, Kanaya Y, Yoshikawa-Inoue H, Irino T, Seki O and Tohjima Y 2019 Environ. Pollut. **247** 55–63

12. Uranishi K, Ikemori F, Shimadera H, Kondo A and Sugata S 2019 Environ. Pollut. **244** 414–22
13. Uranishi K, Ikemori F, Shimadera H, Kondo A and Sugata S 2020 J. Jpn. Soc. Atmos. Environ. **55** 34–49
14. Kaiser J W, Heil A, Andreae M O, Benedetti A, Chubarova N, Jones L, Morcrette J-J, Razinger M, Schultz M G, Suttie M and van der Werf, G R 2012 Biogeosciences **9** 527–54
15. Van der Werf G R, Randerson J T, Giglio L, Van Leeuewn TT, Chen Y, Rogers B M, Mu M, Van Marle M J, Morton D C, Collatz G J and Yokelson R J 2017 Earth System Science Data 2017 **9** 697–720
16. Wiedinmyer C, Kimura Y, McDonald-Buller E C, Emmons L K, Buchholz R R, Tang W, Seto K, Joseph M B, Barsanti K C, Carlton A G and Yokelson R J 2023 Geosci. Model Dev. **16** 3873–91
17. Feng Z, Jun W, Charles I, Edward J H, Zhifeng Y, Cui Y G, Shenjian S, Xiaoyang, Z, Shobha K, Johannes W K, Christine W and Arlindo da S 2014 Environ. Res. Lett. **9** 075002
18. Willmott C J 1981 Phys. Geogr 2 184-94A. Mecke, I. Lee, J.R. Baker jr., M.M. Banaszak Holl, B.G. Orr, Eur. Phys. J. E **14**, 7 (2004)